Mon. Not. R. Astron. Soc. **274**, 256–264 (1995)

The three-dimensional structure of the ISM in front of supernova 1987A

J. Spyromilio,[1,2] D. F. Malin,[1] D. A. Allen,[1] C. J. Steer[3] and W. J. Couch[3]

[1] *Anglo-Australian Observatory, PO Box 296, Epping NSW 2121, Australia*
[2] *European Southern Observatory, Karl-Schwarzschild-Strasse 2, D-85748, Garching, Germany*
[3] *School of Physics, University of New South Wales, PO Box 1, Kensington NSW 2033, Australia*

Accepted 1994 December 3. Received 1994 October 17; in original form 1994 July 7

ABSTRACT

The expanding light echoes surrounding SN 1987A have been studied photographically over a period exceeding 3 yr, sufficiently long that a view of the three-dimensional nature of the reflecting material can now be derived. We present two different projections of the dust distribution. We find a number of discrete clouds, a linear formation and two prominent sheets of material, one of which is clearly split while the other has significant depth. We find an association with the H II region N157C, but *not* with the supergiant shell that forms part of the N157C complex, which we show to lie behind the supernova. Although we still prefer to assign the major echoes to the front and rear faces of a single, uncatalogued supergiant shell, we cannot preclude the existence of two foreground supergiant shells, one inside the other and both containing the supernova. We discuss the association of the echoes with absorption features and recommend further observations that can clarify the structure of this region of the LMC.

Key words: supernovae: individual: SN 1987A – ISM: general – Magellanic Clouds.

1 INTRODUCTION

Supernova 1987A has provided a unique opportunity to derive the three-dimensional structure of the foreground interstellar medium (ISM) in the LMC. The reflection of light emitted from the supernova by material away from the line of sight was observed as early as 1 yr after the explosion (Crotts 1988; Gouiffes et al. 1988; Suntzeff et al. 1988). These light echoes were initially seen as arcs in CCD images of the region surrounding the supernova. Spectra of the arcs confirmed that the reflected light was emitted from the supernova at the time of its maximum brightness, approximately three months after explosion (Gouiffes et al. 1988; Suntzeff et al. 1988; Cannon 1990).

Photographic observations from the AAT taken in 1988 July first demonstrated that the observed arcs, ~40 and ~65 arcsec from the supernova, were in fact complete rings centred approximately on the supernova (Couch, Allen & Malin 1990; hereinafter CAM). Those observations were the first of a programme to monitor the light echoes and investigate the three-dimensional structure of the ISM in the foreground to SN 1987A. Here we report further observations of the light echoes. The data are converted to spatial maps in Section 3 and the three-dimensional information they provide is then examined in Section 4. A discussion of our results can be found in Section 5.

2 OBSERVATIONS AND DATA REDUCTION

The field of SN 1987A was photographed at the $f/3.3$ prime focus of the AAT using the triplet corrector at the epochs given in Table 1. The observing technique was identical to that described in CAM. From all images, we photographically subtracted a plate of the same field obtained at the AAT 3 yr prior to the explosion of SN 1987A (see CAM). This photographic subtraction was described in CAM, although improvements have been made by the use of unsharp masking (Malin 1977). All images have been reconstructed at a scale of 5 arcsec mm^{-1}. The images are reproduced in plates A, B, D, E, F, G, I, J and K (Figs 1–3, opposite p. 258). The digitized data are available from the AAO archive.

The subtracted images were digitized using the AAO PDS and the same technique as CAM with pixels 0.25 arcsec square. The data were further reduced using software developed within the FIGARO data reduction package (Shortridge 1993). To allow a simple determination of the geometry of the intersecting material, the coordinate system of our observations (angular size, position angle and epoch of observation) was converted to a conventional Cartesian coordinate system with the supernova at the origin and the z-axis pointing towards Earth.

The light echoes at any given epoch lie where the ellipsoidal surface of equal light traveltime to the observer inter-

Table 1. Photographic log.

Image	plate numbers	date	emulsion	passband	age (days since maximum light)	averaged seeing (arcsec)
A	2582	1988 July 15	IIaD	V	420	1.5
B	2590,2592	1989 February 6	IIaD,098-04	V,R	626	2.0
D	2632,2633,2643,2644	1989 August 25	IIaD,098-04	V,R	826	1.5
E	2653,2654	1989 October 24	IIaD,098-04	V,R	886	3.0
F	2670,2671	1989 November 21	IIaD	V	914	1.5
G	2677,2688,2689	1990 February 19	IIaD	V	1004	2.0
H	2701	1990 August 24	IIaD	V	1190	2.0
I	2706,2707,2708	1990 December 14	IIaD	V	1302	1.5
J	2726,2727,2728	1991 February 18	IIaD	V	1368	2.0
K	2769,2770,2771	1992 January 3	IIaD	V	1687	1.2

sects matter capable of scattering the light towards the observer. The ellipsoid of constant light traveltime has the Earth and the supernova at the foci and takes the form:

$$\frac{[(D/2)-z]^2}{(D+t)^2/4}+\frac{r^2}{(2Dt+t^2)/4}=1 \qquad (1)$$

where D is the distance to the supernova (in units of light days), t is the elapsed time between the maximum light epoch and the observation of the light echo (in d), and both the physical radius of the ring, r and the z coordinate are measured in light days. We also have $r=(D-z)\tan\theta$, where θ is the angular size of the ring in rad. For the angular sizes considered here we may use

$$r=(D-z)\,\theta. \qquad (2)$$

The light scattered by the ISM left the supernova during the period of maximum light. Following Gouiffes et al. (1988) and Suntzeff et al. (1988), we deem the maximum to have occurred on 1987 May 22, and hence derive the values of the age, t, given in Table 1.

3 CONVERSION TO SPATIAL MAPS

We sought to explore the three-dimensional structure of the scattering material. As Figs 1–3 (opposite p. 258) illustrate, the structures are too complex to be analysed using Couderc's (1939) approximation of a simple inclined sheet. Thus we have identified pixels within each image that can be attributed to reflecting material, and from the x and y coordinates of each pixel relative to the supernova we derive θ and hence z, using equations (1) and (2).

This procedure cannot, unfortunately, be performed automatically. It is impossible to convolve different photographs to the same seeing prior to subtraction, and hence residual star images remain. These are easily differentiated from real echoes by eye, since they remain fixed on the plates. Thus we have had to select representative pixels manually at each epoch.

Although the echoes appear to represent complete rings, the interruption caused by the superposition of residual star images upon the echoes has produced instead a series of unconnected points in space. We found it helpful to group these points into what we believe to be connected structures. We did so on the basis of repeatability of features over successive epochs, and angular extent. Eight groupings were chosen; these are marked on Fig. 4. In the text below we use the numbers on that figure (in bold face) to identify features. We note that, although they appear in our images, we have chosen to ignore the inner echoes seen by Bond et al. (1990) since these have already been discussed extensively by other authors.

We emphasize the arbitrary nature of our pixel selection. In particular, we have tried to give separate identities to all unequivocal cases of splitting of echoes. Where echoes were broad but not split with any certainty, we chose pixels to cover the full range of radius present. Broad sections of echoes therefore appear more prominent. So, too, do isolated but repeatable features (**3**, **4**, **5** and part of **8**), where again we have selected more pixels.

Because the bright phase of the supernova was protracted, some contribution to the apparent width of the rings is produced by the spread of values of t in equation (1). For an infinitely thin sheet perpendicular to the line of sight, a range of 30 d in t (approximately the FWHM of the peak in the light curve) corresponds typically ($z=250$ pc and $t=1000$ d) to an angular extent of less than 1.3 arcsec. For the same typical values a sheet 30 light days wide along the line of sight would result in a 3.3-arcsec echo. The size of the echo on the plane of the sky is further complicated in the case of inclined sheets.

The narrowest echoes seen on Figs 1–3 are of order 1-arcsec FWHM and may result from very thin sheets inclined to the line of sight. Other echoes show widths of order 5 arcsec. The widths of these echoes reflect a large physical thickness of the sheets of dust responsible for them.

4 THE THREE-DIMENSIONAL STRUCTURE OF THE ECHOES

4.1 The view from outside the echoes

We now consider the echoes in a Cartesian coordinate system x, y and z, where the supernova lies at the origin, x increases to the west and y to the north on the sky, and z is measured along the sight line from the supernova. All units are in light days. To measure orientations we use the angle ϕ defined in the usual Cartesian sense ($\tan\phi=y/x$), so that the astronomical definition of position angle is given by $270+\phi$.

The three-dimensional nature of the data necessitates their presentation in a variety of ways. A natural first expectation is that the scattering material occupies thin sheets.

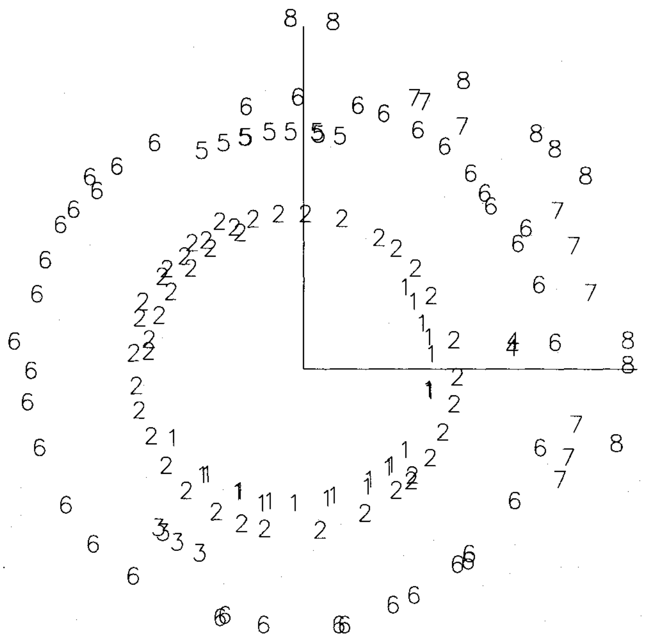

Figure 4. The regions of image I selected as coherent structures. Image I exhibits almost all features present in other images. The numbering sequence is used throughout this paper to describe individual echoes.

Since the extent to which they have been sampled in the x, y direction is small compared to the separation of the sheets, we might expect them to approximate to planes even if they have spherical surfaces created by isotropic outflows from a central source. Hence we can determine the plane of each sheet by rotating the data until the echo appears as a linear feature.

In Fig. 5 we display all observations of all echoes for all epochs, as viewed from within the plane of the sky. We do so at a range of values of ϕ from $-90°$ to $+90°$. The algebraic representation of this rotation is given in Appendix A1. It is immediately apparent that, contrary to previous claims, no structure is perpendicular to the line of sight to the supernova. The two major families of echoes both show inclinations of order 45° to the line of sight, but the orientation of maximum inclination, ϕ, differs for the two. The inner set, echoes **1** and **2**, are seen edge-on when $\phi \sim 40°$, whereas the outer set (**6**, **7**) are edge-on for $\phi \sim 0$.

Most of the other echoes give the impression of being compact, though often elongated, clouds. The outermost echo (**8**), however, may also be a sheet. It accounts for the scatter of points at the right-hand end of Fig. 5. These points appear to form a plane that is seen edge-on at $\phi \sim 20°$. The plane so defined is very steeply inclined to the line of sight, lying almost parallel to it. We suspect that this may indeed be a correct interpretation. Inspection of the plates shows that echo **8** was not seen on early data, and has never formed a complete circle on the sky. If this echo is formed by a sheet of material then the sheet does not extend to both sides of the ellipsoid of constant light traveltime and has an edge. When viewed face-on ($\phi \sim -75°$ in Fig. 5) it appears open-ended to the observer. This behaviour can be explained by the expansion of the ellipsoid of constant traveltime into such a surface.

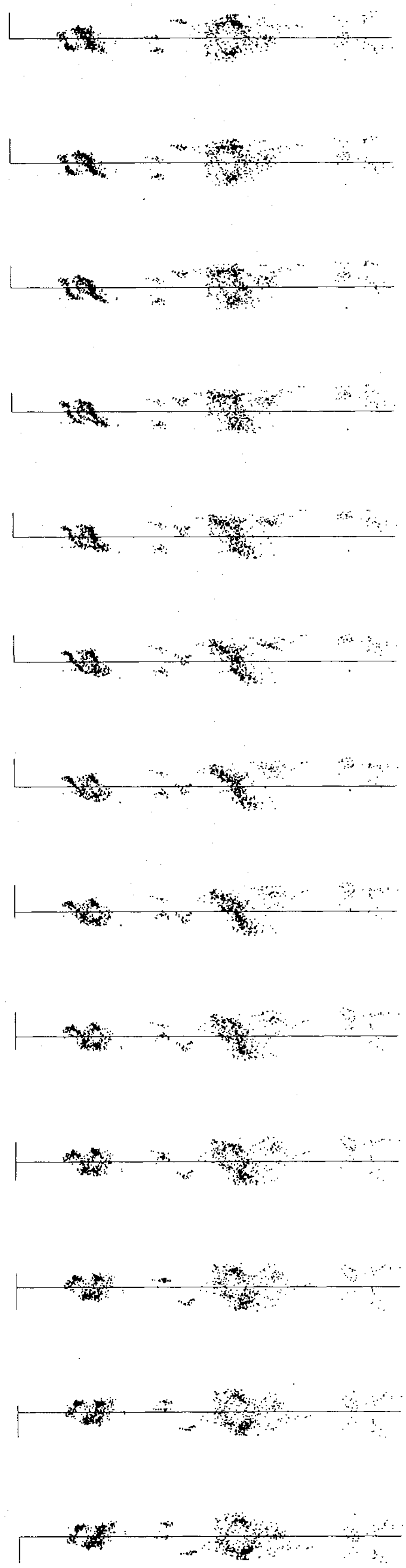

Figure 5. The echoes as seen from within the plane of the sky. A sequence of increasing orientation angles (ϕ) is shown, from $\phi = -90°$ at the bottom, incrementing by 15° to $+90°$ at the top. All epochs are plotted together in this diagram. The supernova is at the origin.

1995MNRAS.274..256S

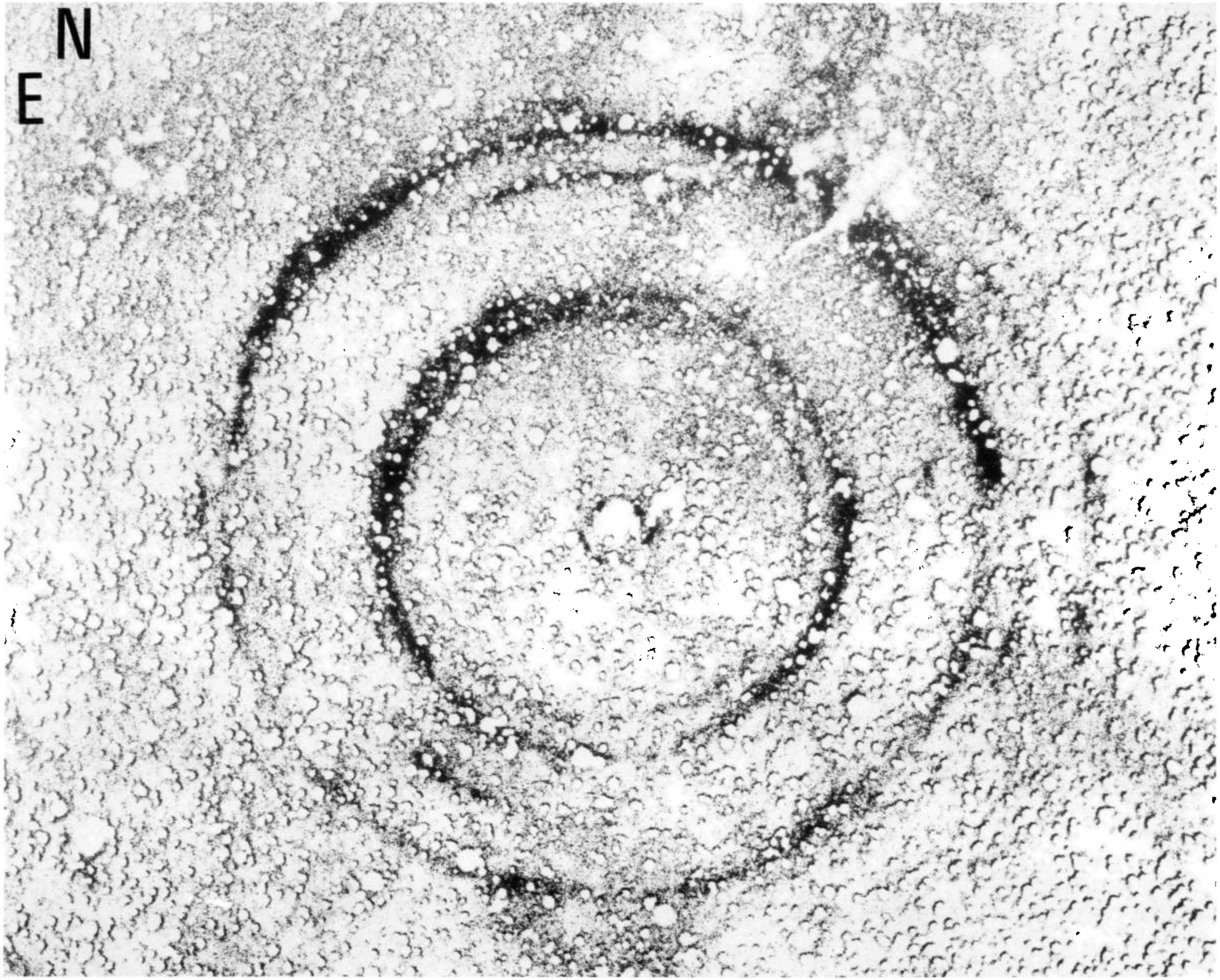

Figure 1. Plate I.

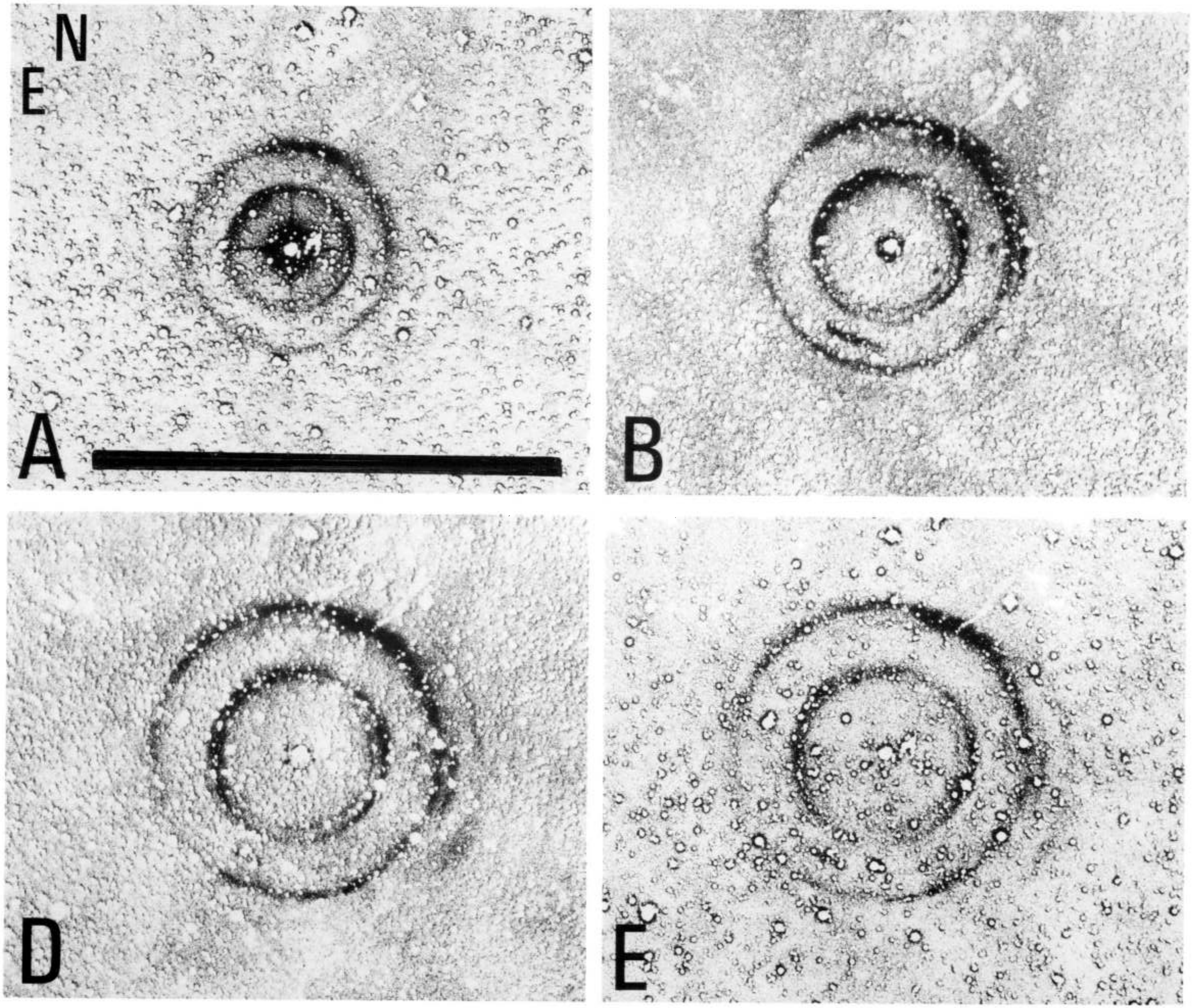

Figure 2. Plates A, B, D and E. Scale bar = 5 arcmin.

1995MNRAS.274..256S

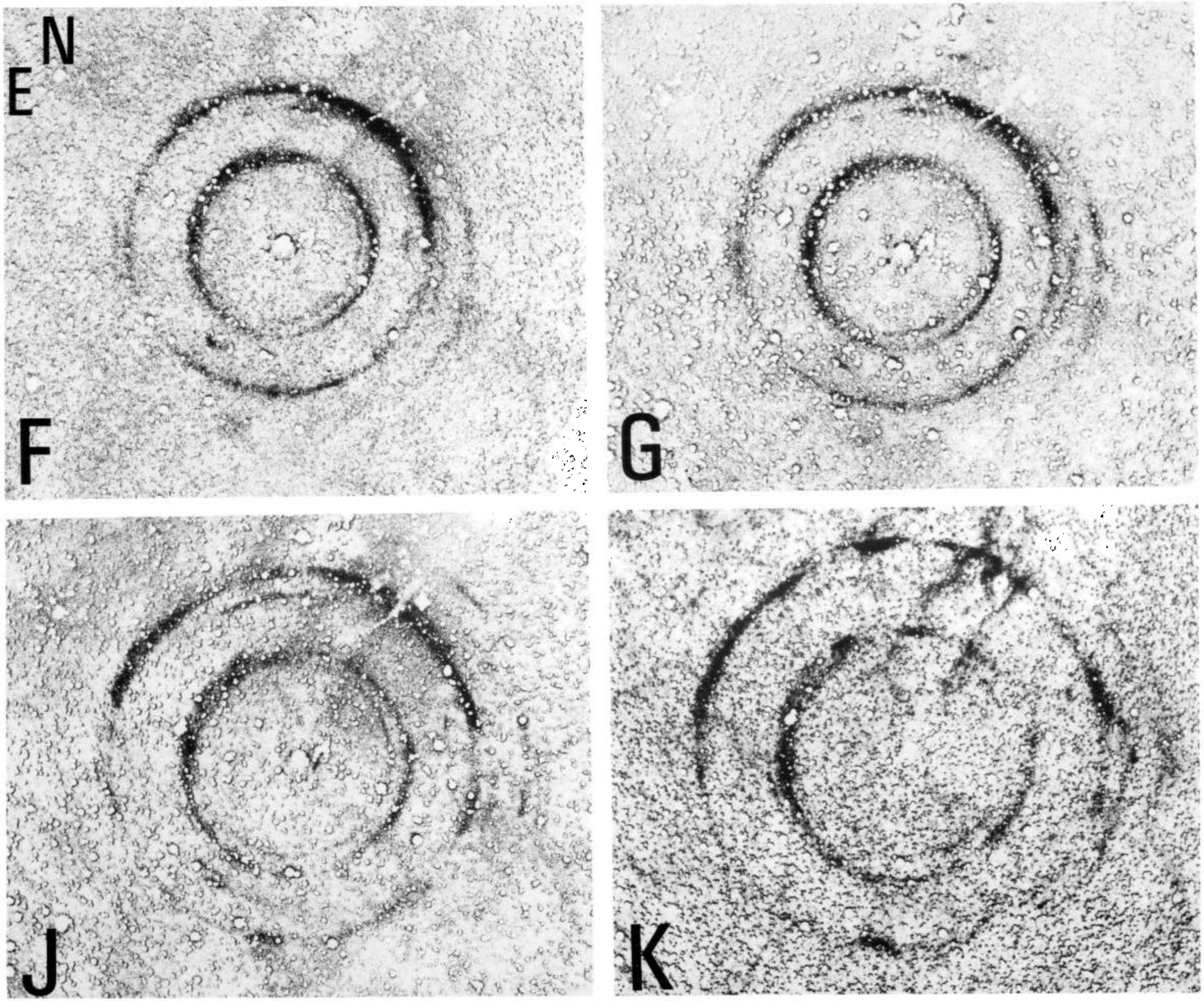

Figure 3. Plates F, G, J and K.

4.2 The view from within the echoes

While Fig. 5 gives a clear picture of the basic structure of the material producing the echoes, it is not well suited to studying individual sheets in detail. We therefore consider a second projection in which we transport the origin to the centre of an echo ($z=\bar{z}$) and define spherical coordinates with z as the vector joining the poles. To project this to two dimensions we ignore radius, and consider latitude as a function of longitude (see Appendix A2). On such a plot, an inclined plane is mapped to a sine curve whose amplitude corresponds to the inclination of the plane. If the echo expands with time along a true plane, data from different epochs will lie on top of one another. If we now rotate the spherical coordinate system, we can bring an inclined plane on to the equator, whereupon it will appear as a straight line on the plot, allowing a precise representation of any warps.

Figs 6–8 display echoes **1**, **2** and **6** in this format, respectively. In each diagram the upper panel has the polar vector along the line of sight while the lower sets it to our best estimate of the normal to the echo.

Echoes **1** and **2** (collectively referred to in other works as the inner ring) are reasonably parallel and can be interpreted as a split in a common sheet. We treat them as part of the same structure.

In Figs 6–8 each selected pixel for each epoch is displayed. A different symbol is used for each epoch. The positional uncertainties in identifying a pixel as a member of a particular echo are about 1 arcsec. The spread of the points displayed is much greater than those positional errors. The upper panels allow a simple three-dimensional visualization of each echo. We encourage readers to replicate the figures on to transparencies and roll them into cylinders so that the sides of the rectangular box meet. The axis of the cylinder thus generated lies along the sight line to the supernova.

The lower panels show the result of rotating the polar vector of the spherical coordinates to lie normal to the plane. The angular rotation required can be determined from either the geometry used in Fig. 5 or that used in Figs 6–8, and the best-fitting values for each echo are listed in Table 2.

5 DISCUSSION

5.1 Correspondence to emission nebulosity

Can we identify features of the Large Magellanic Cloud (LMC) that might correspond to the echoes? In general, sheets of material are evident only in profile where they form bright rims. Viewed face-on they appear as diffuse clouds, giving no clue to their depth along the line of sight, and may be too tenuous to detect.

Some of the nebulous features of this region can be specifically excluded by the absence of intensity enhancements where the echoes cross them. A large arc seen to the south of and concave towards SN 1987A (also visible in image K) is now internal to the echoes, as is most of the honeycomb structure first noticed by Wang (1992). We can therefore position the honeycomb behind the outer echo. Assuming the large arc to be due to limb brightening of the bubble then the fact that the outer echo has overtaken the bubble places the entire structure behind the supernova. As the echoes expand, more information about the position of these structures will be obtained.

To the north and west, substantial nebulosity can be seen even in our subtracted images. This is the brightest portion of N157C, associated with the tight cluster of stars NGC 2044 = LH 90 (Lortet & Testor 1984). N157C contains some bright rims, as discussed by Lortet & Testor, including a bubble blown by a WN3 star that lies outside the range of the echoes to date (see also Malin & Allen 1990 for images showing the nebulosity associated with this region). It was suggested by Crotts (1988) and CAM that the two principal echoes arise in the front and rear surfaces of the large, wind-blown bubble that Lortet & Testor associated with N157C. Wind-blown bubbles have been studied by Meaburn (1980) and Georgelin et al. (1983). The N157C bubble is defined primarily by the bright rim to the south. This is the feature noted above that has already been traversed by the outer echo and therefore cannot form it. The bubble identified by Lortet & Testor is *not* the source of the echoes.

Echo **6**, however, is significantly brighter in the north, suggesting an association between it and the bright, diffuse portion of N157C, as suggested by Crotts (1988). The correspondence between N157C and the light echoes is not perfect. In particular, the NNW portion of the echo has faded even though it continued to intersect both of the obvious ridges of emission in that location. In the NE the echo remained bright, implying a stronger correlation there between the material illuminated by the supernova and N157C. A credible interpretation would identify echo **6** with the H II region seen prominently in the western part of N157C, but recognizes that additional background nebulosity exists along the same line of sight.

We conclude that the large bubble inferred by Lortet & Testor from the bright rim to the south is not associated with the bright H II region to the west, and that the latter is responsible for echo **6**.

5.2 Comparison with supergiant shells

In the following discussion we assume that flat sheets are unlikely configurations and that each echo forms part of a crudely spherical surface. It follows that each bubble must produce one echo if the supernova lies inside it, and two if it lies behind.

Fig. 5 clearly shows that the normals to the two major echoes, **1** + **2** and **6**, drawn through the areas sampled, cannot intersect. This precludes them forming opposite sides of a single spherical surface, for such a structure would produce planes with opposite inclinations at the same position angle.

However, spherical bubbles are not the norm. The detailed structure within the echoes is on the scale of Meaburn's giant shells ~ 50 pc (1 pc = 1190 light days), while the scale of the entire echo pattern is comparable to his supergiant shells (~ 100–500 pc). Random cuts through the shells shown in Davies, Elliott & Meaburn (1976) have much the same character as Fig. 5, including the spatial separations of the shell walls and the angles made by cuts by tangents to those shells. We infer that the material causing the echoes is distributed in a similar way to the supergiant shells, with significant warping from spherical.

If, indeed, the major echoes **1** + **2** and **6** form coherent surfaces on the scale of the supergiant shells, then two different configurations can be considered. Either they form the front and rear faces of a single shell, or there are two shells in

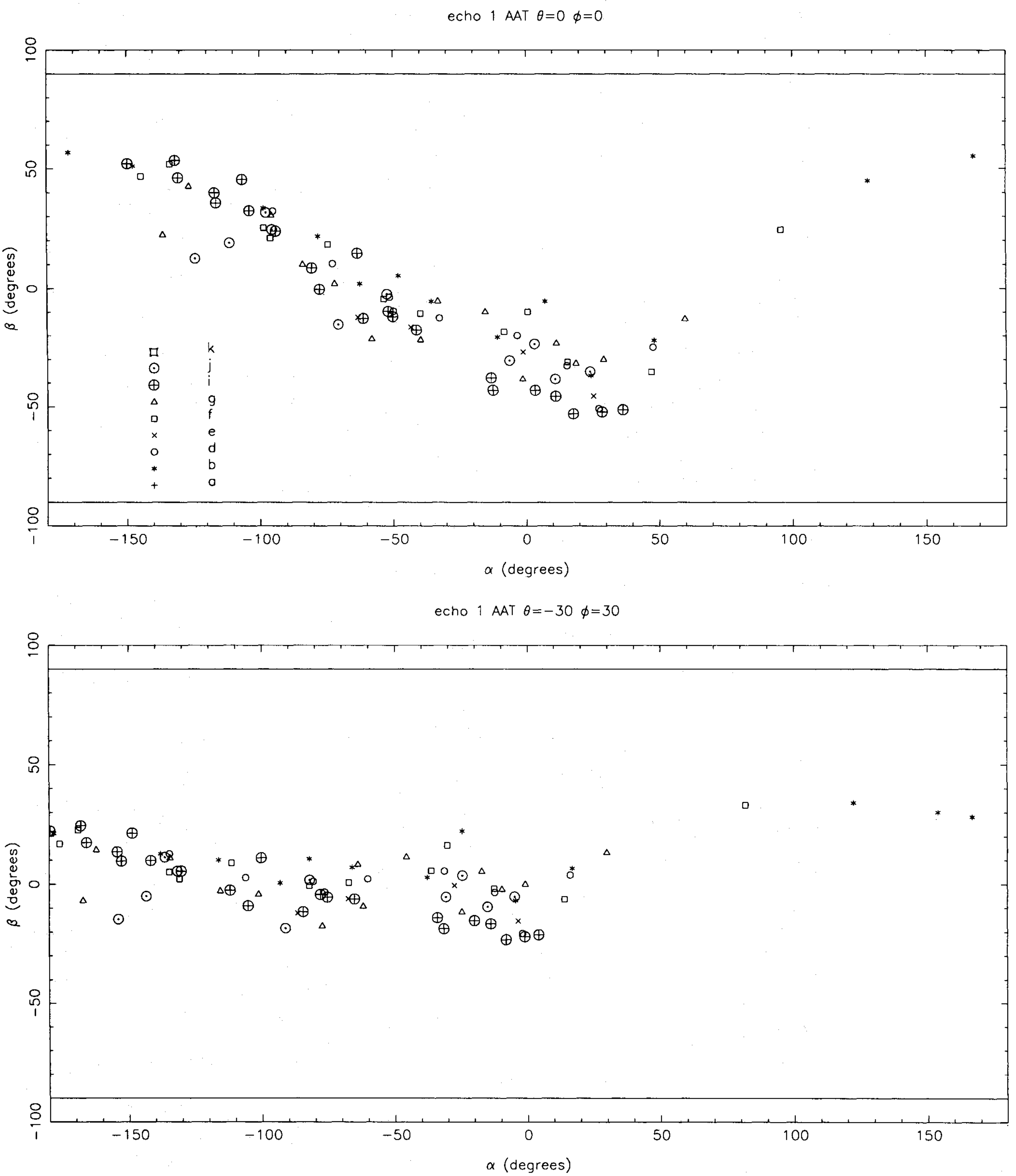

Figure 6. Sky maps of echo 1 for an observer within its plane and on the line of sight between the supernova and the Earth. In the upper panel the spherical projection assumes that the poles lie along the Earth–SN direction. In the lower plot the polar vector lies normal to the best-fitting plane.

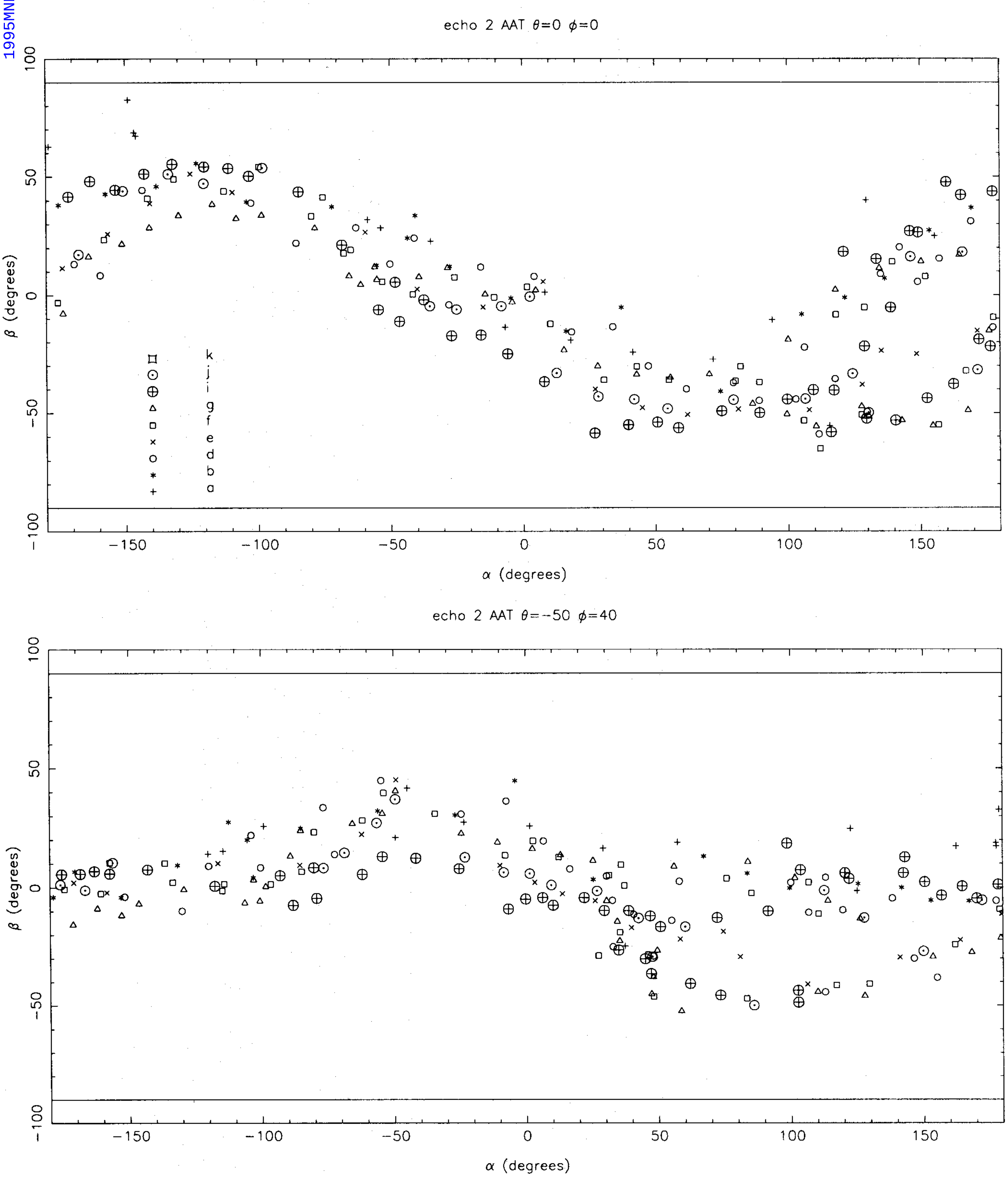

Figure 7. As Fig. 6, for echo **2**.

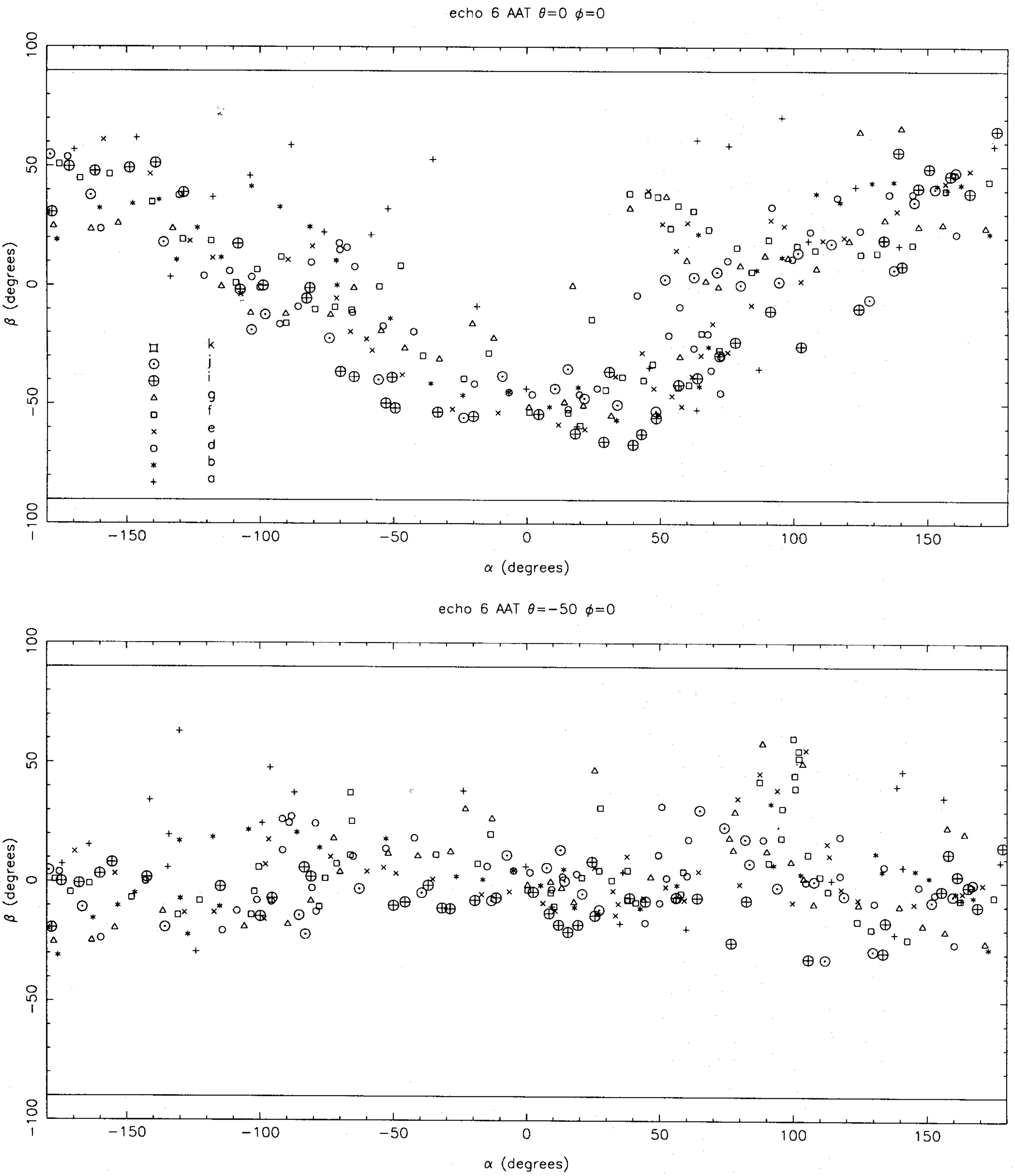

Figure 8. As Fig. 6, for echo **6**.

Table 2. Echo parameters.

echo ID	ϕ	θ	mean distance (pc)
1	30	-30	90
2	40	-50	125
3			235
4			235
5			275
6	0	-50	350
7			410
8			520

each of which we observe only one wall. In the latter case, if the second surface were closer to us than the supernova, we would expect to have seen its echo, and so we require the second, rear surface of both to lie behind SN 1987A, and the shells to reside one inside the other.

In favour of two unrelated shells is the absence of strong curvature in the shell walls. For the outer echo, we find a minimum radius of curvature of 180 pc (40 arcmin), which can be compared to the separation of the sheets of 260 pc. This is, however, a weak constraint given the non-spherical nature of supergiant shells. It should be noted that the bright rim in N157C that lies beyond the supernova has the wrong curvature for it to be one of the two shells, so that there would be three large shells along the line of sight.

Favouring a single supergiant shell is the fact that at all stages except A (15/7/88) both major echoes showed clear evidence of splitting over almost the same range of position angle, and with somewhat similar relative intensities for the two components. This was first pointed out by CAM. Features **1** and **2** represent the splitting of the inner echo, which has persisted. Echo **6** has rarely formed two completely separate entities, because the split became filled; it is not represented by the increased breadth of the echo.

We cannot prove either configuration. We believe, however, that a single shell is the more credible choice, if only because of the statistical unlikelihood of the sight line intercepting two shells, within both of which lies SN 1987A.

Whichever configuration is correct, an important implication of our data is that *compact gas/dust clouds exist within swept-up shells*. These could be dense knots in the interstellar medium that resisted passage of the wind-blown shell, but we would expect them to have retained moderate density and thus to be especially bright. Alternatively, they may represent material ejected subsequently by mass-loss stars.

5.3 Absorption features due to the echo sheets

All scattering material along the line of sight which extends more than a few arcsec perpendicular to that line should have been observed as a light echo. We would thus have expected to record the material responsible for the interstellar absorption features observed in the spectra of SN 1987A. D'Odorico, Molaro & Vladilo (1991) observed the interstellar Na D lines towards SN 1987A and the two companion stars. Two components are present towards SN 1987A at velocities of +220 and +280 km s^{-1} (the velocity of SN 1987A is 287 km s^{-1}; Meikle et al. 1991). However, only the +280 km s^{-1} component is observed towards the other two stars, which lie a few arcsec from SN 1987A, but at quite unknown distances along the line of sight.

We would very much like to assign the two absorption features to the two major echoes. If we do not make this assignment, then we must invoke two dust-rich gas clouds producing echoes but no Na I absorption, and two separate gas-rich clouds producing absorption and no echoes, an unlikely situation. For our preferred configuration of a single, expanding supergiant shell, the 220 km s^{-1} absorption would originate in the nearer surface (echo **6**). Such an assignment would imply an expansion speed of 30 km s^{-1}, and a minimum age for the shell of 4×10^6 yr. Velocities higher than this have been recorded in some supergiant shells (e.g. Meaburn, Terrett & Blades 1981), so there is no incompatibility.

What inhibits this interpretation is the absence of the 220 km s^{-1} feature in absorption in the spectra of the two companion stars to SN 1987A. This result requires either that thin portions of the shell are aligned with the companion stars but not the supernova, so that the companions lie in front of the 220 km s^{-1} echo and are aligned so closely with the supernova by chance. Both of these are very unlikely. The latter configuration also implies that the 280 km s^{-1} gas lies to the front, and that the two echoes are not formed by a single expanding shell.

D'Odorico et al. suggest that the 220 km s^{-1} absorption arises in an innermost echo, dubbed Napoleon's hat (Wang & Wampler 1992), located only a few arcsec from and physically very close to the supernova and which we do not discuss here. This readily allows the two companion stars to lie in front of the cloud, but precludes the two echoes being identified with the two absorption features.

There is clearly a need to examine more thoroughly the absorption spectra towards not only the companion stars, but also a number of other stars in the region. A velocity map of N157C is also of particular interest.

Gas at coronal temperatures has been recorded through its absorption in [Fe X] (Pettini et al. 1989). Their interpretation strongly favoured a supergiant shell ionized by ancient supernovae, and they associated that shell with 30 Dor. An association with NGC 2044 does not seem to be precluded.

The velocity range of the absorption, 215–270 km s^{-1}, is in striking agreement with the sodium absorption features. This appears to provide strong evidence that the two prominent absorption features correspond to opposite sides of a hot, expanding shell, and strengthens our assignment of the echoes to the front and rear faces of that shell.

5.4 Location of SN 1987A in the LMC

The scaleheight of the old stellar population of the LMC is 500 pc (Freeman, Illingworth & Oemler 1983), while that of the younger population, from which the progenitor of SN 1987A would have originated, may well be a factor of 2 smaller. We have argued that the N157C bubble lies behind the supernova. In the echoes we are seeing material extending in front of SN 1987A by a large fraction of the depth of the LMC. It follows that SN 1987A probably lies close to the mean plane of the LMC and is therefore a reliable distance indicator for the galaxy.

ACKNOWLEDGMENTS

We thank ATAC and the Director, AAO for their long-term support of this programme. We also thank the anonymous referee for many valuable comments.

REFERENCES

Bond H. E., Gilmozzi R., Meakes M. G., Panagia N., 1990, ApJ, 354, L49
Cannon R. D., 1990, in Protheroe R. J., ed., Proc. 21st International Cosmic Ray Conf., 12, 1, University of Adelaide, Adelaide
Couch W. J., Allen D. A., Malin D. F., 1990, MNRAS, 242, 555 (CAM)
Couderc P., 1939, Ann. d'Astrophys., 2, 271
Crotts A. P. S., 1988, ApJ, 333, L51
Davies R. D., Elliott K. H., Meaburn J., 1976, Mem. R. Astron. Soc., 81, 89
D'Odorico S., Molaro P., Vladilo G., 1991, A&A, 247, L5
Freeman K. C., Illingworth G., Oemler A., 1983, ApJ, 272, 488
Georgelin Y. M., Georgelin Y. P., Laval A., Monnet G., Rosado M., Artier N., Lombard J., Viale A., 1983, A&AS, 54, 459
Gouiffes C. et al., 1988, A&A, 198, L9
Lortet M. C., Testor G., 1984, A&A, 139, 330
Malin D. F. M., 1977, Am. Astron. Soc. Photogr. Bull., 16, 10
Malin D. F. M., Allen D. A., 1990, Sky Telesc., 79, 23
Meaburn J., 1980, MNRAS, 192, 365
Meaburn J., Terrett D. L., Blades J. C., 1981, MNRAS, 197, 19
Meikle W. P. S., Cumming R. J., Spyromilio J., Allen D. A., Mobasher B., 1991, in Danziger I. J., Kjar K., eds, Supernova 1987A and Other Supernovae. ESO Garching, p. 595
Pettini M., Stathakis R., D'Odorico S., Molaro P., Vladilo G., 1989, ApJ, 340, 256
Shortridge K., 1993, in Hanisch R. J., Brissenden R. J. V., Barnes J., eds, Astronomical Data Analysis Software and Systems II. Astron. Soc. Pac., San Francisco, p. 219
Suntzeff N. B., Heathcote S., Weller W. G., Caldwell N., Huchra J. P., Olowin R. P., Chambers K. C., 1988, Nat, 334, 135
Wang L., 1992, Messenger, 69, 34
Wang L., Wampler E. J., 1992, A&A, 262, L9

APPENDIX A1: COORDINATE SYSTEM USED IN FIG. 5

We first rotate the data about the z axis by an angle ϕ and then about the newly created y axis by the angle ψ. Suppose we consider a point with initial coordinates (x_0, y_0, z_0). Then, following these manipulations, its coordinates (y_1, z_1) will be given by

$$y_1 = x_0 \sin\phi + y_0 \cos\phi,$$

$$z_1 = z_0 \cos\psi - (x_0 \cos\phi - y_0 \sin\phi) \sin\psi.$$

In Fig. 5, $\psi = 0$, z_1 is plotted along the abscissa and y_1 along the ordinate.

APPENDIX A2: COORDINATE SYSTEM USED IN FIGS 6–8

The coordinate system is rotated about the z axis by angle ϕ:

$$x_1 = x_0 \cos\phi - y_0 \sin\phi,$$

$$y_1 = x_0 \sin\phi + y_0 \cos\phi,$$

$$z_1 = z_0 - z_{\mathrm{ave}}.$$

The new coordinate system is then rotated about the new x axis (θ) giving the new coordinate system (x_2, y_2, z_2):

$$x_2 = x_1,$$

$$y_2 = z_1 \sin\theta + y_1 \cos\theta,$$

$$z_2 = z_1 \cos\theta - y_1 \sin\theta,$$

On the abscissae of Figs 6–8 we display angle α, where

$$\alpha = \tan^{-1} \frac{x_2}{y_2},$$

and, along the ordinates, angle β, where

$$\beta = \tan^{-1} \frac{z_2}{\sqrt{x_2^2 + y_2^2}}.$$